

# Generation of Terahertz Radiation via the Transverse Thermoelectric Effect

Petar Yordanov, Tim Priessnitz,\* Min-Jae Kim, Georg Cristiani, Gennady Logvenov, Bernhard Keimer, and Stefan Kaiser\*

Terahertz (THz) radiation is a powerful tool with widespread applications ranging from imaging, sensing, and broadband communications to spectroscopy and nonlinear control of materials. Future progress in THz technology depends on the development of efficient, structurally simple THz emitters that can be implemented in advanced miniaturized devices. Here, it is shown how the natural electronic anisotropy of layered conducting transition metal oxides enables the generation of intense terahertz radiation via the transverse thermoelectric effect. In thin films grown on off-cut substrates, femtosecond laser pulses generate ultrafast out-of-plane temperature gradients, which in turn launch in-plane thermoelectric currents, thus allowing efficient emission of the resulting THz field out of the film structure. This scheme is demonstrated in experiments on thin films of the layered metals PdCoO<sub>2</sub> and La<sub>1.84</sub>Sr<sub>0.16</sub>CuO<sub>4</sub>, and model calculations that elucidate the influence of the material parameters on the intensity and spectral characteristics of the emitted THz field are presented. Due to its simplicity, the method opens up a promising avenue for the development of highly versatile THz sources and integrable emitter elements.

## 1. Introduction


Miniaturization of functional components is crucial for the realization of integrated terahertz ( $\approx 0.1$ – $30$  THz) technology.<sup>[1]</sup>

P. Yordanov, T. Priessnitz, M.-J. Kim, G. Cristiani, G. Logvenov, B. Keimer, S. Kaiser

Max Planck Institute for Solid State Research  
Heisenbergstraße 1, 70569 Stuttgart, Germany  
E-mail: t.priessnitz@fkf.mpg.de; stefan.kaiser@tu-dresden.de

T. Priessnitz, M.-J. Kim, S. Kaiser  
4th Physics Institute and Research Center SCoPE  
University of Stuttgart  
Pfaffenwaldring 57, 70569 Stuttgart, Germany

M.-J. Kim, S. Kaiser  
Institute of Solid State and Materials Physics  
TUD Dresden University of Technology  
Haeckelstraße 3, 01069 Dresden, Germany

 The ORCID identification number(s) for the author(s) of this article can be found under <https://doi.org/10.1002/adma.202305622>

© 2023 The Authors. Advanced Materials published by Wiley-VCH GmbH. This is an open access article under the terms of the Creative Commons Attribution-NonCommercial-NoDerivs License, which permits use and distribution in any medium, provided the original work is properly cited, the use is non-commercial and no modifications or adaptations are made.

DOI: 10.1002/adma.202305622

In particular, advances in THz emitters are driven by the discovery of new materials and generation mechanisms that enable their integration into compact circuit modules. Currently, portable sources of intense THz radiation commonly rely on external femtosecond laser oscillators. The most widely used designs utilize ultrafast currents of photoexcited charge carriers in semiconductors (photoconductive antennas) or optical rectification (OR) in nonlinear crystals.<sup>[2,3]</sup> In view of the growing number of applications of THz technology, however, researchers are pursuing a diverse set of strategies to devise new concepts for THz sources with optimal efficiency, size, ease of fabrication, flexibility regarding operating conditions, and compatibility with various planar hybrid structures. Recent pertinent examples include spintronic emitters based on ultrafast photoexcitation of spin currents in ferromagnetic–nonmagnetic metallic multilayers,<sup>[4–9]</sup> and quantum cascade lasers operating at elevated temperatures.<sup>[10]</sup>

## 2. Methods

Here, we take advantage of the intrinsic thermopower anisotropy of naturally layered materials and the properties of the transverse thermoelectric effect (TTE) (see Supporting Information).<sup>[11–24]</sup> We report on the light-induced generation of large ultrafast charge currents by an ultrafast TTE. Driving these currents in off-cut grown thin films of layered transition metal oxides allows for efficient THz generation and simple device structures (Figure 1a). The method operates with monolithic thin films without the need for heteroepitaxy or extensive processing, and implies virtually no restrictions of the operating conditions. We consider the metallic delafossite PdCoO<sub>2</sub> (Figure 1a) due to its exceptionally high quasi-2D in-plane electrical conductivity, large thermal diffusivity, and anisotropic thermopower,<sup>[25–31]</sup> and show how this combination of properties establishes the basis of a new, versatile, and highly scalable method for the generation of THz radiation. The comparison to the layered anisotropic cuprate La<sub>2–x</sub>Sr<sub>x</sub>CuO<sub>4</sub> ( $x = 0.16$ ) identifies the nonequilibrium carrier diffusion in the ultrafast TTE as key element defining the THz emission properties. Thin-film samples were prepared and

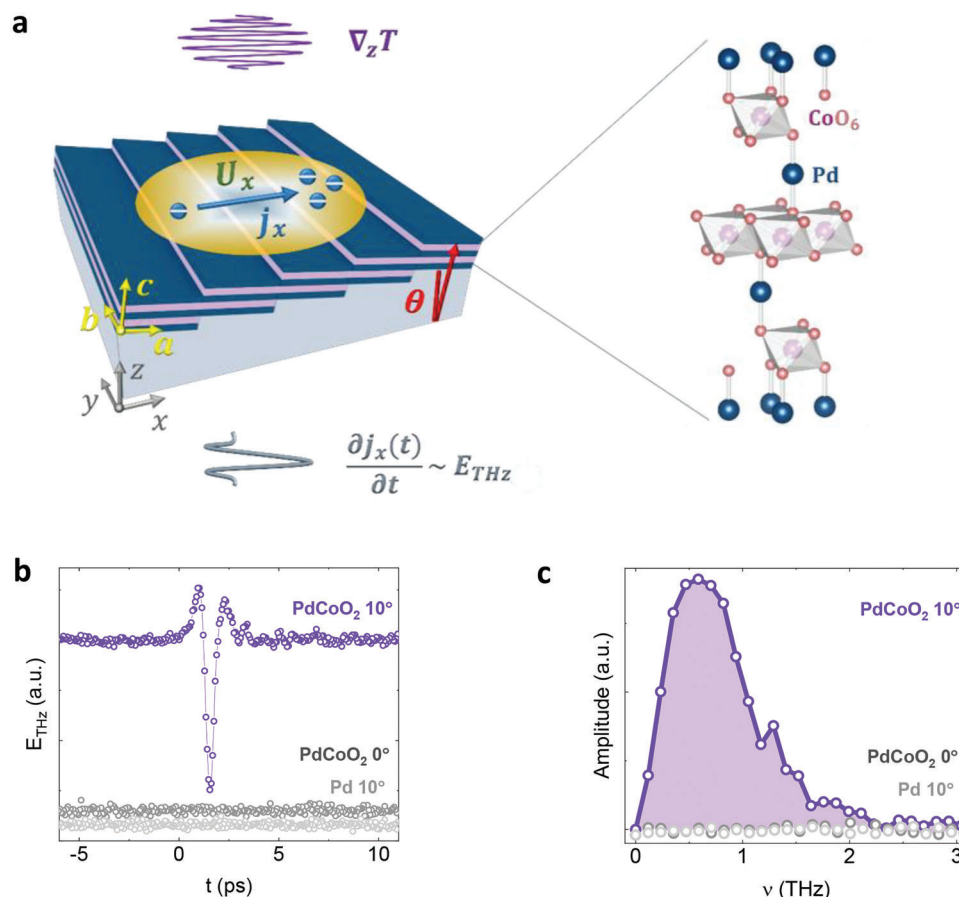


**Figure 1.** Generation of terahertz radiation via the transverse thermoelectric effect. a) Thin film of a material with anisotropic Seebeck coefficient deposited on an off-cut substrate for TTE-driven THz generation. Inset: Crystal structure of the delafossite PdCoO<sub>2</sub>, comprising metallic Pd and insulating CoO<sub>2</sub> layers, with highly anisotropic structural and transport properties.<sup>[25–36]</sup> b) Electric field strength and c) amplitude spectrum emitted from a thin film ( $d \approx 10$  nm) of PdCoO<sub>2</sub> on a  $\theta = 10^\circ$  off-cut Al<sub>2</sub>O<sub>3</sub> substrate, as described in the text. Reference measurements on a PdCoO<sub>2</sub> film grown on a regular  $\theta = 0^\circ$  Al<sub>2</sub>O<sub>3</sub> substrate, and on an elemental Pd film on a  $\theta = 10^\circ$  Al<sub>2</sub>O<sub>3</sub> substrate are also shown.

characterized as described in the Experimental Section and detailed for PdCoO<sub>2</sub> in ref. [32].

Upon laser excitation, the TTE generates a thermoelectric field  $E_x$ , proportional to the difference of the Seebeck coefficients ( $\Delta S = S_{ab} - S_c$ ) and perpendicular to the temperature gradient ( $E_x \perp \nabla_z T$ ), in layered materials with anisotropic Seebeck coefficients ( $S_a = S_b \equiv S_{ab} \neq S_c$ ) (Figure 1a). Heating a layer with thickness of the order of the optical penetration depth  $\delta_{opt,z}$ , the ultra-short laser pulse induces a temperature gradient  $\nabla_z T = \Delta T_z/d$ , where  $\Delta T_z$  is the temperature difference between the front and the back side of the film and  $d$  is the film thickness.<sup>[18]</sup> In return,  $\Delta T_z$  activates a directed thermal diffusion of mobile charge carriers along the  $x$ -axis resulting in the thermoelectric field  $E_x$ /voltage  $U_x$ , respectively. The heating profile consists of two components, an ultrafast heating of the electronic system and a subsequent heating of the lattice due to thermalization of hot electrons interacting with the lattice. Picosecond-changes to the corresponding ultrafast diffusion current give rise to THz emission.

### 3. Results and Discussion

Figure 1b shows the emitted single-cycle THz response  $E_{THz}(t)$  from exciting a thin film of PdCoO<sub>2</sub> deposited on  $\theta = 10^\circ$  off-cut substrate using  $\tau_{lp} \approx 250$  fs optical laser pulses at a fluence of  $F_{lp} = 0.5$  mJ cm<sup>-2</sup> where the detection is performed in a standard electro-optical sampling (EOS) scheme in ZnTe. The corresponding amplitude spectrum in Figure 1c reveals a relatively broad bandwidth of  $\nu \approx 0.1$ –2.3 THz with a peak amplitude at  $\nu \approx 0.6$  THz.

To understand the origin of THz generation, we turn to laser-induced thermoelectric voltage (LITV) experiments. These show that an efficient TTE can be realized in thin films deposited on special off-cut substrates, so that the  $c$ -axis grows at an angle  $\theta \neq 0^\circ, 90^\circ$  relative to the surface normal (see Supporting Information).<sup>[1–5]</sup> The induced transverse thermoelectric field and voltage become

$$U_x = E_x l = \frac{l}{d} \frac{\sin 2\theta}{2} (S_{ab} - S_c) \Delta T_z \quad (1)$$

for a laser spot diameter  $l$  and where  $E_x$  and  $U_x$  are the components due to the TTE (directed along the projection of the tilted  $c$ -axis on the film surface).<sup>[11]</sup>  $E_y$  and  $U_y$  equal zero by symmetry.  $E_z$  and  $U_z$  are described by the conventional thermoelectric Seebeck effect.

The aspect ratio  $l/d$  enhances  $U_x$  by a factor of  $\approx 10^4$  to  $10^5$  compared to the conventional longitudinal response  $U_z$ . The voltage dynamics  $U_x(t)$  is determined by the characteristic time for heat diffusion through the film,  $\tau_r \sim d^2/D_z$ , where  $D_z = \kappa_z/\rho_m c_p$  is the thermal diffusivity,  $\kappa_z$  is the thermal conductivity,  $\rho_m$  is the density, and  $c_p$  is the specific heat of the material.<sup>[14]</sup> The corresponding time-dependent electric current density in the plane of the film,  $j_x(t) \sim U_x(t)/\rho_x$  where  $\rho_x$  is the effective electrical resistivity, gives rise to the  $z$ -axis-directed dipole emission in the THz domain,  $E_{\text{THz}}(t) \sim \partial j_x(t)/\partial t$ ,<sup>[37]</sup> if  $\tau_r \lesssim 1$  ps and the laser pulses are sufficiently short ( $\tau_{\text{lp}} \lesssim \tau_r$ ).

For PdCoO<sub>2</sub> at room temperature, the resistivity is  $\rho_{\text{ab}}/\rho_c \approx 2.6/1070 \mu\Omega \text{ cm}$ ,<sup>[26,27]</sup> the thermal conductivity is  $\kappa_{\text{ab}}/\kappa_c \approx 300/50 \text{ W K}^{-1} \text{ m}^{-1}$ ,<sup>[29]</sup> and the thermal diffusivity is  $D_{\text{ab}}/D_c = 1.1 \times 10^{-4}/1.8 \times 10^{-5} \text{ m}^2 \text{ s}^{-1}$ .<sup>[33]</sup> Recent experiments on PdCoO<sub>2</sub> thin films and powder compacts supported the theoretical predictions for the thermopower showing  $S_{\text{ab}}/S_c \approx 4/(-30) \mu\text{V K}^{-1}$ , i.e., a difference of  $\Delta S = (S_{\text{ab}} - S_c) \approx 34 \mu\text{V K}^{-1}$ , at room temperature.<sup>[32–34]</sup> We used pulsed laser deposition to synthesize films with  $d \approx 10$  nm and  $0^\circ \leq \theta \leq 25^\circ$  on optically transparent Al<sub>2</sub>O<sub>3</sub> substrates.<sup>[32,34,35]</sup> Measurements of the transverse voltage  $U_x(t)$  induced by UV laser pulses with  $\tau_{\text{lp}} \approx 5$  ns yielded a substantial amplitude and negligible broadening of the voltage signal, thus providing direct confirmation of the large thermopower anisotropy in PdCoO<sub>2</sub> and indicating a characteristic response time  $\tau_r \ll 5$  ns for the films (see Supporting Information). However, dynamics in our ultrafast excitation scheme is expected on much faster timescales and will define the excitation spectrum. Electronic heating is likely to happen within our 250 fs excitation pulse while lattice heating typically occurs on picosecond-timescales.<sup>[38]</sup> The observed THz emission and the bandwidth of 2.3 THz indicate that the thermal anisotropy already builds up on these ultrafast timescales.

To prove that this THz generation is based on the TTE-mechanism, we measure the absence of THz emission from films of PdCoO<sub>2</sub> on regular  $\theta = 0^\circ$  substrate and elemental Pd on  $\theta = 10^\circ$  off-cut substrate (Figure 1b,c).  $E_{\text{THz}}(t)$  cancels completely at  $\theta = 0^\circ$ , which is consistent with Equation (1), and excludes an emission due to the ordinary Seebeck effect along the  $z$ -axis.<sup>[39]</sup> The absence of signal from the Pd film on  $\theta = 10^\circ$  off-cut substrate eliminates other possible sources of THz radiation related to the specific step-terrace film structure. Moreover, this effectively also rules out surface field effects as the primary mechanism for the observed THz generation. While surface field-related THz emission is primarily found in semiconductors, where built-in electric fields at the surface drive a charge separation leading to subsequent THz emission, our metallic transition metal oxide thin film lacks the characteristic bandgap and surface electric fields found in semiconductors. This makes surface field effects unlikely to be the primary cause of THz emission in our system. Additionally, the significant discrepancy in characteristic length scales between our system (20 nm) and a study on surface plasmons (200 nm), assuming a linear relation between wavevector and

plasma frequency, further supports the exclusion of surface field effects as the primary cause of THz emission in our specific case.<sup>[32,40]</sup>

To foster the TTE origin of the THz generation, we also conduct sample orientation-dependent measurements under normal incidence as shown in Figure 2a,b. For the thermoelectric origin of the THz emission, a  $\varphi = 180^\circ$  rotation of the sample around the surface normal  $\vec{n}$ , switches the sign of the polarity of the measured field  $E_{\text{THz}}$ . Flipping the sample, i.e., changing from front- to reverse-side illumination, results in the same polarity switch as it effectively changes the direction of the terrace structure (tiled  $c$ -axis). Combining both steps restores the initial polarity of the THz field. In detail, this can be understood by looking at Equation (1). The current  $j_x \sim U_x/R_x$ , where  $R_x$  is the electrical resistance, and therefore the field  $E_{\text{THz}} \sim \partial j_x/\partial t$ , switches direction and polarity, respectively, upon  $\theta \rightarrow -\theta$  or  $\Delta T_z \rightarrow -\Delta T_z$  exchange.  $\theta \rightarrow -\theta$  is equivalent to the sample rotation by an angle  $\varphi = 180^\circ$  around the surface normal  $\vec{n}$ , while  $\Delta T_z \rightarrow -\Delta T_z$  is realized by the sample flip. At the same time, due to the symmetry of the tilted crystalline structure, this front-to-back-side change of perspective is also equivalent to  $\theta \rightarrow -\theta$ , and hence, effectively,  $\Delta T_z \rightarrow -\Delta T_z$  does not lead to a switch of the current  $j_x$  direction nor of the  $E_{\text{THz}}$  polarity.

Further, since the TTE is highly anisotropic, the currents are restricted along the  $x$ -axis (Equation (1)). Thus, the generated THz field is linearly polarized as shown by a  $90^\circ$ -oscillating signal amplitude upon sample rotation  $\varphi$  about  $\vec{n}$ , at fixed pump pulse polarization  $P_{\text{pump}}$  and polarizer position  $P_{\text{pol}}$  (Figure 2c,d). The absence of a pump polarization  $P_{\text{pump}}$  dependence of the emitted THz signal (Figure 2e) rules out optical rectification mechanisms in the THz generation,<sup>[41]</sup> and demonstrates the primary role of the laser pulse as a heat source.

Having firmly established the TTE mechanism of THz generation, we now present the results of additional experiments aimed at gaining a more in-depth understanding of the factors influencing the amplitude and spectral characteristics of the emitted THz field. Figure 3a,b displays data from thin films of PdCoO<sub>2</sub> deposited on  $\theta = 10^\circ$ ,  $15^\circ$ , and  $25^\circ$  off-cut substrates. A clear trend of declining peak field and spectral amplitude at larger  $\theta$  is visible, indicating that the increase of the thermoelectric voltage  $U_x$  with  $\theta$  up to  $45^\circ$  predicted by Equation (1) is overcompensated by the  $\theta$ -dependences of the other effective quantities contributing to the THz source currents  $j_x$  and field  $E_{\text{THz}}$  (see Supporting Information).

To gain further insight into the influence of materials parameters, we have studied TTE-induced THz generation in thin films of the layered metal La<sub>1.84</sub>Sr<sub>0.16</sub>CuO<sub>4</sub> (LSCO), whose thermopower anisotropy is comparable to that of PdCoO<sub>2</sub> ( $\Delta S \approx 40 \mu\text{V K}^{-1}$ ) while its electrical resistivity is substantially higher ( $\rho_{\text{ab}}/\rho_c \approx 150/30\,000 \mu\Omega \text{ cm}$ ) and its thermal diffusivity an order of magnitude lower ( $D_{\text{ab}}/D_c \approx 3 \times 10^{-6}/1.5 \times 10^{-6} \text{ m}^2 \text{ s}^{-1}$ ).<sup>[21,42–44]</sup> Figure 3 shows that the spectrum emitted from an LSCO film with  $d \approx 10$  nm and  $\theta = 15^\circ$  is qualitatively similar to the corresponding PdCoO<sub>2</sub> data, which suggests that the TTE mechanism is common to layered metal oxides. The different materials parameters are reflected in a reduced THz field strength and enhanced spectral range compared to PdCoO<sub>2</sub>, highlighting the potential of materials exploration in the development of functional devices.

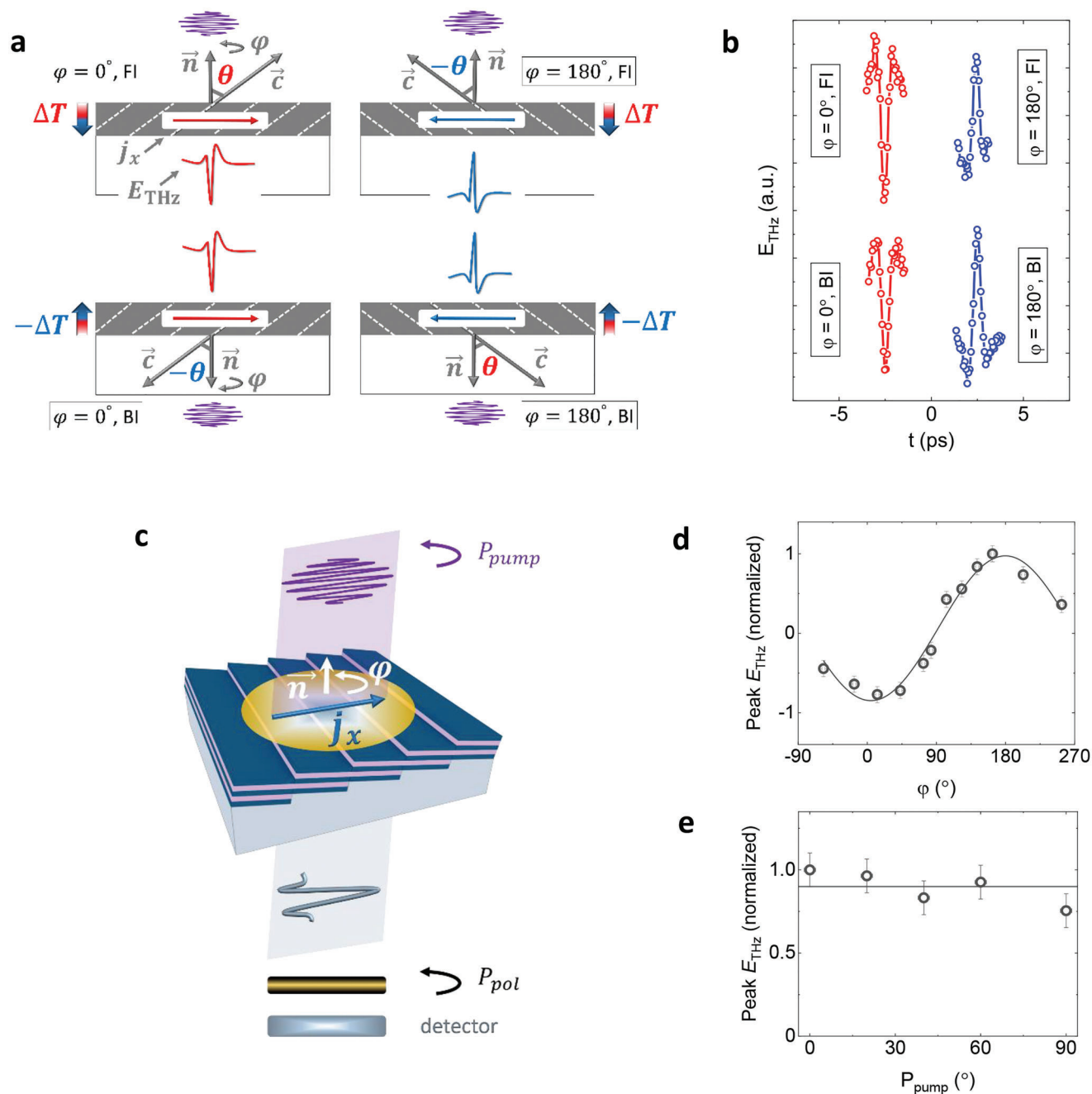


**Figure 2.** Confirmation of the TTE mechanism for THz generation. a) Current density ( $j_x$ ) direction and electric field ( $E_{\text{THz}}$ ) polarity upon  $\varphi = 0^\circ \rightarrow 180^\circ$  rotation about the surface normal  $\vec{n}$  (equivalent to  $\theta \rightarrow -\theta$  in Equation (1)) (left to right), and upon change from front side (FI) to backside (BI) illumination (equivalent to a combined operation of both  $\Delta T_z \rightarrow -\Delta T_z$  and  $\theta \rightarrow -\theta$  in Equation (1)) (top to bottom). b) Experimental  $E_{\text{THz}}(t)$  waveforms emitted from the PdCoO<sub>2</sub> film in the four different configurations in (a). c) Experimental setup to investigate the polarization state of the emitted THz field and the dependence on the pump polarization. d) Normalized peak THz electric field as a function of  $\varphi$  for fixed pump polarization  $P_{\text{pump}} = 0^\circ$  and polarizer angle  $P_{\text{pol}} = 0^\circ$ . The line denotes a sinusoidal fit of the data points. Note that  $\varphi = 180^\circ$  is defined as the maximum of the sinusoidal fit. e) Normalized peak THz electric field as a function of the pump polarization  $P_{\text{pump}}$ , for fixed  $\varphi = 0^\circ$  and  $P_{\text{pol}} = 0^\circ$ . The horizontal line is a guide to the eye and indicates the behavior expected if the intensity does not depend on  $P_{\text{pump}}$ . The error bars show the standard deviation of the noise.

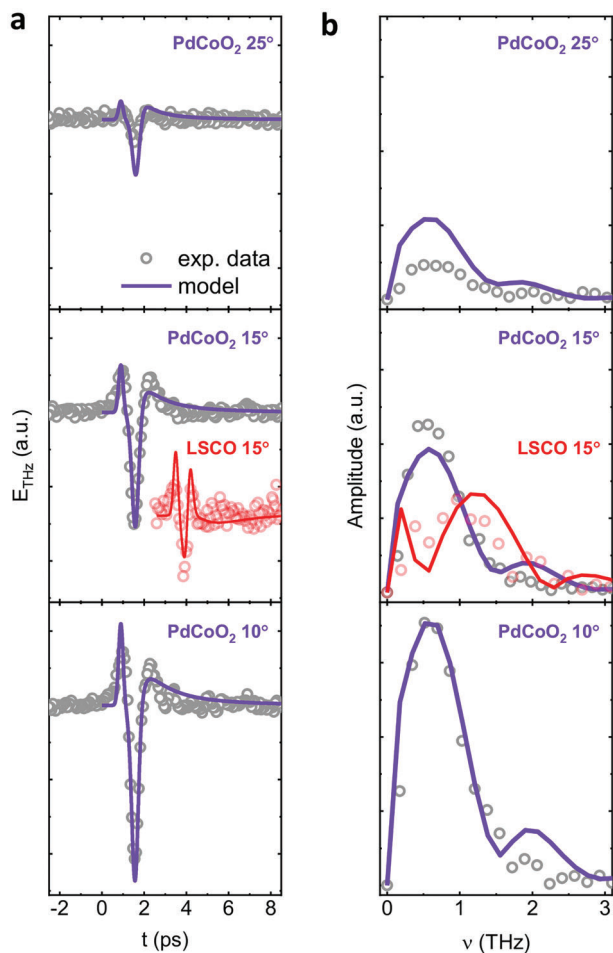


**Figure 3.** Experimental data and model calculations of TTE-THz generation in thin films of PdCoO<sub>2</sub> and La<sub>1.84</sub>Sr<sub>0.16</sub>CuO<sub>4</sub>-off-cut angle dependence. a,b) Experimental (light gray and light red) and calculated (violet and red) THz field  $E_{\text{THz}}(t)$  (a) and amplitude spectra (b) from PdCoO<sub>2</sub> and La<sub>1.84</sub>Sr<sub>0.16</sub>CuO<sub>4</sub> (LSCO) films with  $d \approx 10$  nm on substrates with different off-cut angles. The THz field  $E_{\text{THz}}(t)$  from the La<sub>1.84</sub>Sr<sub>0.16</sub>CuO<sub>4</sub> (LSCO) film is shown with an offset for clarity.

Guided by these observations, we have devised a simple model for the THz far field,  $E_{\text{THz}}(t) \sim [1/(1 + n_z)] \times \partial j_x(t)/\partial t$ ,<sup>[37]</sup> where  $n_z$  refers to the refractive index at THz frequencies, in response to the thermoelectric voltage calculated according to Equation (1), with the full set of anisotropic materials parameters for both PdCoO<sub>2</sub> and LSCO (see Supporting Information). Figure 3 shows that the model calculations yield a good description of the key experimental data in both time and frequency domains. Deviations between calculated and measured data for the PdCoO<sub>2</sub> film on a  $\theta = 25^\circ$  substrate are likely a consequence of structural defects that degrade the electronic properties at high off-cut angles. The dominant mechanism which drives the decrease of the peak  $E_{\text{THz}}$  and amplitude at large  $\theta$  is ascribed to the increasing contribution of the more resistive  $c$ -axis transport ( $\rho_{ab} \ll \rho_c$ ) to  $\rho_x$ . Similarly, the reduced THz intensity observed in the LSCO film is explained by the higher overall resistivity of this material compared to that of PdCoO<sub>2</sub>.

An essential component in the model is the transient thermal diffusivity  $D_z^*$ , which depends on the laser pulse duration  $\tau_{\text{lp}}$  and fluence  $F_{\text{lp}}$ , and has been shown to reach values three or more orders of magnitude larger than those in equilibrium.<sup>[45–47]</sup> In metallic systems, the transient thermal diffusivity is expected to thermalize through scattering with a characteristic time  $\tau_{\text{th}}$  that ranges from a few tens to a few hundreds of femtoseconds.<sup>[48]</sup> These experimental findings are significant for TTE-THz generation, because they indicate that manipulation of the laser pulse characteristics can be used not only to manipulate the THz field strength, but also to enhance the thermal diffusivity and extend the THz bandwidth. In the model, we define a time-dependent function of the form  $D_z(t) = D_z^0 + (D_z^* - D_z^0)e^{-t/\tau_{\text{th}}}$  with  $D_z^*$  up to  $5000 \times D_z^0$  and  $\tau_{\text{th}} = 70\text{--}120$  fs, which results in two-component profiles for the temperature difference  $\Delta T_z(t)$  and current density  $j_x(t)$ . The corresponding THz waveforms thus comprise fast transient and slower equilibrium components corresponding to the spectral ranges below and above 0.5 THz, respectively. Whereas this separation of scales is clearly visible in the shape of the spectra of LSCO, the two regimes overlap in PdCoO<sub>2</sub> due to the much higher equilibrium thermal diffusivity. We speculate that the two timescales could well represent fast electronic and slower phononic responses of the system. However detailed insight into the buildup dynamics of the temperature gradients of the sub-systems would require additional measurements that go beyond the scope of this manuscript.

Nevertheless, the model calculations capture key details of the experimentally observed spectra that indicate two time scales and allow us to point out various perspectives for the enhancement of the TTE-driven THz generation. In particular, the optimal value of the off-cut angle  $\theta$  is determined by a complex superposition of contributions from all relevant anisotropic transport coefficients. Based on bulk input model parameters for PdCoO<sub>2</sub>, the maximum of  $E_{\text{THz}}(\theta)$  is expected in the range  $3^\circ \leq \theta \leq 7^\circ$ , which is quite comparable with the trend in the experimental data indicating a peak field at  $\theta \approx 10^\circ$  (see Figure 3a,b and Supporting Information). We attribute the discrepancy to differences between the anisotropy ratios of the material parameters of the bulk (which were used as input for the model calculations) and the thin films. We note that the thickness of the films used in our experiments ( $d = 10$  nm) is well below the optical penetration depth ( $\delta_{ab} \approx 70$  nm,  $\delta_c \approx 100$  nm at wavelength 800 nm),<sup>[36]</sup> so that the pump intensity should be uniform across the film. Nevertheless, our orientation dependent measurements in Figure 2 show that the heat gradient follows the propagation direction of the laser pulse. Details of the transient heat propagation, the lateral heat dissipation, and the influence of the air-film and film-substrate interfaces will require additional measurements. That also includes exploring different substrates as a tuning parameter. Our simple model predicts an enhancement of  $\Delta T_z$  and a corresponding enhancement of  $E_{\text{THz}}$  in the regime  $d > \delta_z$ . While we have thus far been unable to synthesize films of this thickness with sufficient quality, there is obviously a large potential for optimization of PdCoO<sub>2</sub> thin-film systems and for exploration of other layered materials for TTE-driven THz generation.

To put the generated THz field strength into perspective, we performed reference measurements on a commercial ZnTe ((110) orientation,  $d = 1$  mm) optical rectification source whose

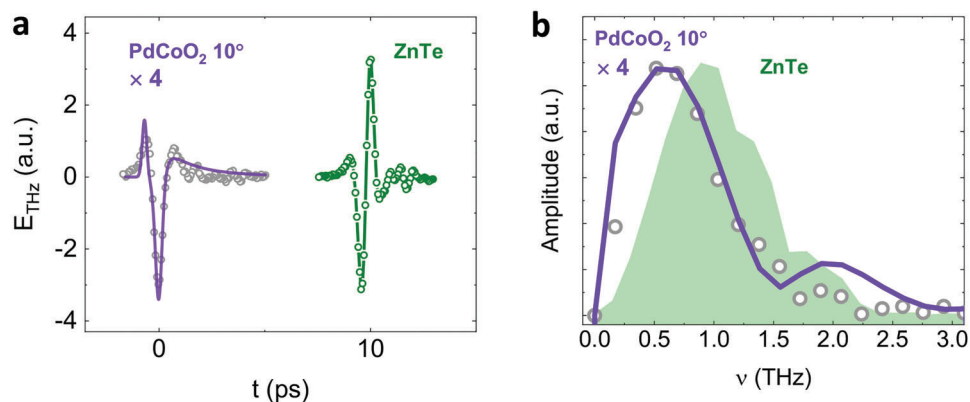


**Figure 4.** Determination of the THz electric field strength. a,b) Comparative plots of the electric field strength (a) and spectra of THz radiation (b) from a  $d = 10$  nm,  $\theta = 10^\circ$  PdCoO<sub>2</sub> film (gray open circles: experimental data, purple lines: model calculations described in the text) and from a ZnTe OR source (experimental data), for  $\tau_{lp} \approx 250$  fs and  $F_{lp} = 0.5$  mJ cm<sup>-2</sup>.

peak field at pump fluence  $F_{lp} = 0.5$  mJ cm<sup>-2</sup> can be expected to be in the range  $E_{THz} \approx 10^5$  to  $10^6$  V m<sup>-1</sup>.<sup>[49,50]</sup> For this experiment, the time-domain THz emission setup was optimized for THz emission from ZnTe via optical rectification. After this the ZnTe crystal was replaced by a PdCoO<sub>2</sub> thin film, and the corresponding THz emission was measured without any further adjustments to the setup. **Figure 4** shows that the amplitude of the radiation emitted from the PdCoO<sub>2</sub> source is only a factor of four lower than the reference source, which implies a peak field strength of  $E_{THz} \approx 10^5$  V m<sup>-1</sup>. The high intensity of the TTE-driven THz emission is remarkable because the PdCoO<sub>2</sub> data were taken on a monolithic, unprocessed film. This finding already indicates a high potential for optimization of the intensity. Comparing the THz emission spectrum from PdCoO<sub>2</sub> with ZnTe (**Figure 4b**) shows the two distinct components arising from the transient and equilibrium diffusivity, whereas ZnTe shows a single optical rectification component. Exploring the bandwidth of the emitter is a subject of future studies. The bandwidth typically depends on various factors, mainly the fluence and pulse length. We note that the limited bandwidth of PdCoO<sub>2</sub> of 2.5 THz shown here is due to the cut-off frequency of ZnTe that is used as EOS crystal.

#### 4. Conclusion

We have shown that the natural anisotropy of the transport properties of layered metal oxides enables the generation of intense THz radiation via the transverse thermoelectric effect. We demonstrated this scheme in thin films of PdCoO<sub>2</sub> and La<sub>1.84</sub>Sr<sub>0.16</sub>CuO<sub>4</sub>, which yielded THz field strengths and spectral bandwidths already comparable to those of commercial ZnTe OR sources. The experimental scheme does not require elaborate fabrication methods and complementary microstructure elements, application of a bias voltage, an external magnetic field, or excessive laser fluence, and it is not limited to a particular material, temperature range, or specific operational conditions. The comparison of two different materials and the complementary model calculations we have reported indicate multiple tuning parameters for manipulation of the intensity and band-

width of the THz field. TTE-THz generation may thus provide a powerful basis for the development of versatile THz sources and single-layer emitter elements. Further intriguing perspectives may emerge from possible static or dynamic interactions of the THz source current and field with various electronic states and correlations, such as high-temperature superconductivity, magnetism, and ferroelectricity, which can be explored by integration of ultrathin films of the emitter material into artificial superlattices with different transition metal oxides.<sup>[51]</sup>

#### 5. Experimental Section

**Thin-Film Synthesis:** Pulsed laser deposition was used to grow PdCoO<sub>2</sub> films with thickness  $d \approx 10$  nm on regular  $c$ -axis-oriented  $\theta = 0^\circ$  (0001) and off-cut  $\theta = 5\text{--}25^\circ$  (0001  $\rightarrow$  11 $\bar{2}$ 0) Al<sub>2</sub>O<sub>3</sub> substrates. The growth conditions included stoichiometric single-phase PdCoO<sub>2</sub> polycrystalline targets, oxygen pressures of 2–3 mbar, a substrate temperature of  $\approx 620$  °C, and laser energy density 1.9 J cm<sup>-2</sup> with repetition rate 3–5 Hz. The film quality was confirmed by X-ray diffraction and high-resolution transmission electron microscopy.<sup>[32]</sup> La<sub>1.84</sub>Sr<sub>0.16</sub>CuO<sub>4</sub> films with  $d \approx 10$  nm on LaSrAlO<sub>4</sub> substrates with off-cut angle  $\theta = 15^\circ$  were synthesized by atomic layer-by-layer ozone-assisted molecular-beam epitaxy (DCA Instruments). The substrate temperature determined by a radiation pyrometer was 650 °C, and the background ozone–oxygen pressure was 10<sup>-5</sup> Torr. The atomic layer-by-layer growth was monitored by using in situ reflection high electron energy diffraction. The film quality was confirmed by high-resolution X-ray diffraction, atomic force microscopy, and scanning transmission electron microscopy.

**Terahertz Emission Spectroscopy:** The measurements were performed by using femtosecond ( $\tau_{lp} \approx 250$  fs) optical pulses (central wavelength  $\lambda_{lp} = 800$  nm) generated by a Ti:sapphire amplifier (Coherent RegA 9000) at a repetition rate of 150 kHz and pump fluence of  $F_{lp} \approx 0.5$  mJ cm<sup>-2</sup> seeded by a Ti:sapphire oscillator (Coherent Mira 900). The THz emission was detected via the EOS method using a ZnTe (110) nonlinear crystal with thickness  $d = 1$  mm, a balancing photodetector, and a lock-in amplifier. In the sample rotation measurements, a wire grid polarizer was used to fix the polarization plane of the detected THz radiation. All measurements were performed at room temperature. The excess 800 nm optical pump after the sample was blocked using a polytertrafluoroethylene plate. The optical pump was focused onto the sample using a lens to a spot size of roughly 1 mm. Off-axis parabolic mirrors were used to collimate and focus the generated THz radiation onto the EOS detection crystal.

## Supporting Information

Supporting Information is available from the Wiley Online Library or from the author.

## Acknowledgements

P.Y. and T.P. contributed equally to this work. The authors acknowledge financial support by the German Research Foundation (Deutsche Forschungsgemeinschaft, DFG, Project No. 107745057 - CRC/TRR 80, subproject G8).

Open access funding enabled and organized by Projekt DEAL.

## Conflict of Interest

P.Y., T.P., M.J.K., B.K., and S.K. are listed as inventors on a patent application (European Patent Office application number EP21172006A) related to the research presented in this article. The patent application is currently pending, and no financial gains or benefits have been received or are anticipated at this time. The other authors declare that they have no financial or nonfinancial competing interests.

## Data Availability Statement

The data that support the findings of this study are available from the corresponding author upon reasonable request.

## Keywords

layered conducting transition metal oxides, off-cut thin films, terahertz generation, THz emission spectroscopy, transverse thermoelectric effect

Received: June 12, 2023

Revised: July 29, 2023

Published online: September 8, 2023

- [1] K. Sengupta, T. Nagatsuma, D. M. Mittleman, *Nat. Electron.* **2018**, *1*, 622.
- [2] J.-A. Fülöp, S. Tzortzakis, T. Kampfrath, *Adv. Opt. Mater.* **2019**, *8*, 1900681.
- [3] P. Shumyatsky, R. R. Alfano, *J. Biomed. Opt.* **2011**, *16*, 033001.
- [4] T. Seifert, S. Jaiswal, U. Martens, J. Hannegan, L. Braun, P. Maldonado, F. Freimuth, A. Kronenberg, J. Henrizi, I. Radu, E. Beaurepaire, Y. Mokrousov, P. M. Oppeneer, M. Jourdan, G. Jakob, D. Turchinovich, L. M. Hayden, M. Wolf, M. Münzenberg, M. Kläui, T. Kampfrath, *Nat. Photonics* **2016**, *10*, 483.
- [5] T. S. Seifert, S. Jaiswal, J. Barker, S. T. Weber, I. Rzdolski, J. Cramer, O. Gueckstock, S. F. Maehrlin, L. Nadvornik, S. Watanabe, C. Ciccarelli, A. Melnikov, G. Jakob, M. Münzenberg, S. T. B. Goennenwein, G. Woltersdorf, B. Rethfeld, P. W. Brouwer, M. Wolf, M. Kläui, T. Kampfrath, *Nat. Commun.* **2018**, *9*, 2899.
- [6] R. Rouzegar, A. L. Chekhov, Y. Behovits, B. R. Serrano, M. A. Syskaki, C. H. Lambert, D. Engel, U. Martens, M. Münzenberg, M. Wolf, G. Jakob, M. Kläui, T. S. Seifert, T. Kampfrath, *Phys. Rev. Appl.* **2023**, *19*, 034018.
- [7] Z. Jin, Y. Peng, Y. Ni, G. Wu, B. Ji, X. Wu, Z. Zhang, G. Ma, C. Zhang, L. Chen, A. V. Balakin, A. P. Shkurinov, Y. Zhu, S. Zhuang, *Laser Photonics Rev.* **2022**, *16*, 2100688.
- [8] Z. Jin, Y. Guo, Y. Peng, Z. Zhang, J. Pang, Z. Zhang, F. Liu, B. Ye, Y. Jiang, G. Ma, C. Zhang, A. V. Balakin, A. P. Shkurinov, Y. Zhu, S. Zhuang, *Adv. Phys. Res.* **2023**, *2*, 2200049.
- [9] K. Ishibashi, S. Iihama, S. Mizukami, *Phys. Rev. B* **2023**, *107*, 144413.
- [10] B. Wen, D. Ban, *Prog. Quantum Electron.* **2021**, *80*, 100363.
- [11] H. Lengfellner, G. Kremb, A. Schnellbögl, J. Betz, K. F. Renk, W. Prettl, *Appl. Phys. Lett.* **1992**, *60*, 501.
- [12] H. Lengfellner, S. Zeuner, W. Prettl, K. F. Renk, *Europhys. Lett.* **1994**, *25*, 375.
- [13] L. R. Testardi, *Appl. Phys. Lett.* **1994**, *64*, 2347.
- [14] S. Zeuner, H. Lengfellner, W. Prettl, *Phys. Rev. B* **1995**, *51*, 11903.
- [15] T. Zahner, R. Stierstorfer, S. Reindl, T. Schauer, A. Penzkofer, H. Lengfellner, *Phys. B* **1999**, *313*, 37.
- [16] H. J. Goldsmid, *J. Electron. Matter.* **2011**, *40*, 1254.
- [17] T. Zahner, R. Schreiner, R. Stierstorfer, O. Kus, S. T. Li, R. Roessler, J. D. Pedarnig, D. Bäuerle, H. Lengfellner, *Europhys. Lett.* **1997**, *40*, 673.
- [18] P. X. Zhang, W. K. Lee, G. Y. Zhang, *Appl. Phys. Lett.* **2002**, *81*, 4026.
- [19] P. X. Zhang, H.-U. Habermeier, *J. Nanomater.* **2008**, *2008*, 329601.
- [20] H.-U. Habermeier, X. H. Li, P. X. Zhang, B. Leibold, *Solid State Commun.* **1999**, *110*, 473.
- [21] F. Xiong, H. Zhang, Z. M. Jiang, P. X. Zhang, *J. Appl. Phys.* **2008**, *104*, 053118.
- [22] L. Yu, Y. Wang, P. Zhang, H.-U. Habermeier, *Phys. Status Solidi RRL* **2013**, *7*, 180.
- [23] K. Takahashi, T. Kanno, A. Sakai, H. Adachi, Y. Yamada, *Appl. Phys. Lett.* **2010**, *97*, 021906.
- [24] K. Takahashi, T. Kanno, A. Sakai, H. Adachi, Y. Yamada, *Phys. Rev. B* **2011**, *83*, 115107.
- [25] R. D. Shannon, D. B. Rogers, C. T. Prewitt, *Inorg. Chem.* **1971**, *10*, 713.
- [26] H. Takatsu, S. Yonezawa, S. Mouri, S. Nakatsuji, K. Tanaka, Y. Maeno, *J. Phys. Soc. Jpn.* **2007**, *76*, 104701.
- [27] C. W. Hicks, A. S. Gibbs, A. P. Mackenzie, H. Takatsu, Y. Maeno, E. A. Yelland, *Phys. Rev. Lett.* **2012**, *109*, 116401.
- [28] P. J. W. Moll, P. Kushwaha, N. Nandi, B. Schmidt, A. P. Mackenzie, *Science* **2016**, *351*, 1061.
- [29] R. Daou, R. Frésard, S. Hébert, A. Maignan, *Phys. Rev. B* **2015**, *91*, 041113.
- [30] K. P. Ong, D. J. Singh, P. Wu, *Phys. Rev. Lett.* **2010**, *104*, 176601.
- [31] M. E. Gruner, U. Eckern, R. Pentcheva, *Phys. Rev. B* **2015**, *92*, 235140.
- [32] P. Yordanov, W. Sigle, P. Kaya, M. E. Gruner, R. Pentcheva, B. Keimer, H.-U. Habermeier, *Phys. Rev. Mater.* **2019**, *3*, 085403.
- [33] P. Yordanov, A. S. Gibbs, P. Kaya, S. Bette, W. Xie, X. Xiao, A. Weidenkaff, H. Takagi, B. Keimer, *Phys. Rev. Mater.* **2021**, *5*, 015404.
- [34] B. Geisler, P. Yordanov, M. E. Gruner, B. Keimer, R. Pentcheva, *Phys. Status Solidi B* **2022**, *259*, 2100270.
- [35] T. Harada, *Mater. Today Adv.* **2021**, *11*, 100146.
- [36] C. C. Homes, S. Khim, A. P. Mackenzie, *Phys. Rev. B* **2019**, *99*, 195127.
- [37] J. Shan, T. F. Heinz, in *Ultrafast Dynamical Processes in Semiconductors*, (Ed: K.-T. Tseng), Topics in Physics, Vol. 92 Springer, Berlin/Heidelberg, Germany, **2004**, pp. 1–567.
- [38] L. Cheng, Q.-B. Yan, M. Hu, *Phys. Chem. Chem. Phys.* **2017**, *19*, 21714.
- [39] K. Takahashi, T. Kanno, A. Sakai, H. Tamaki, H. Kusada, Y. Yamada, *Adv. Opt. Mater.* **2014**, *2*, 428.
- [40] S. Macis, L. Tomarchio, S. Tofani, F. Piccirilli, M. Zacchigna, V. Aglieri, A. Toma, G. Rimal, S. Oh, S. Lupi, *Commun. Phys.* **2022**, *5*, 145.
- [41] V. L. Malevich, R. Adomavičius, A. Krotkus, *C. R. Phys.* **2008**, *9*, 130.
- [42] Y. Nakamura, S. Uchida, *Phys. Rev. B* **1993**, *47*, 8369.
- [43] J.-Q. Yan, J.-S. Zhou, J. B. Goodenough, *New J. Phys.* **2004**, *6*, 143.
- [44] C. H. Mousatov, S. A. Hartnoll, *npj Quantum Mater.* **2021**, *6*, 81.
- [45] E. Najafi, V. Ivanov, A. Zewail, M. Bernardi, *Nat. Commun.* **2017**, *8*, 15177.
- [46] N. Gedik, J. Orenstein, R. Liang, D. A. Bonn, W. N. Hardy, *Science* **2003**, *300*, 1410.

- [47] A. Block, A. Principi, N. C. H. Hesp, A. W. Cummings, M. Liebel, K. Watanabe, T. Taniguchi, S. Roche, F. H. L. Koppens, N. F. van Hulst, K.-J. Tielrooij, *Nat. Nanotechnol.* **2021**, *16*, 1195.
- [48] B. Y. Mueller, B. Rethfeld, *Phys. Rev. B* **2013**, *87*, 035139.
- [49] T. Löffler, T. Hahn, M. Thomson, F. Jacob, H. G. Roskos, *Opt. Express* **2005**, *13*, 5353.
- [50] F. Blanchard, L. Razzari, H.-C. Bandulet, G. Sharma, R. Morandotti, J.-C. Kieffer, T. Ozaki, M. Reid, H. F. Tiedje, H. K. Haugen, F. A. Hegmann, *Opt. Express* **2007**, *15*, 13212.
- [51] H. Y. Hwang, Y. Iwasa, M. Kawasaki, B. Keimer, N. Nagaosa, Y. Tokura, *Nat. Mater.* **2012**, *11*, 103.